AIP Advances

Measuring the complex field scattered by single submicron particles

Marco A. C. Potenza, Tiziano Sanvito, and Alberto Pullia

Citation: AIP Advances **5**, 117222 (2015); doi: 10.1063/1.4935927

View online: http://dx.doi.org/10.1063/1.4935927

View Table of Contents: http://scitation.aip.org/content/aip/journal/adva/5/11?ver=pdfcov

Published by the AIP Publishing

Measuring the complex field scattered by single submicron particles

Marco A. C. Potenza,[1,2,3,a] Tiziano Sanvito,[1,2,3] and Alberto Pullia[1]
[1]*Department of Physics, University of Milan, via Celoria, 16 – I-20133 Milan, Italy*
[2]*CIMAINA, University of Milan, via Celoria, 16 – I-20133 Milan, Italy*
[3]*EOS s.r.l., viale Ortles 22/4, I-20139 Milan, Italy*

(Received 21 July 2015; accepted 4 November 2015; published online 11 November 2015)

We describe a method for simultaneous measurements of the real and imaginary parts of the field scattered by single nanoparticles illuminated by a laser beam, exploiting a self-reference interferometric scheme relying on the fundamentals of the Optical Theorem. Results obtained with calibrated spheres of different materials are compared to the expected values obtained through a simplified analytical model without any free parameters, and the method is applied to a highly polydisperse water suspension of Poly(D,L-lactide-co-glycolide) nanoparticles. Advantages with respect to existing methods and possible applications are discussed. [http://dx.doi.org/10.1063/1.4935927]

I. INTRODUCTION

Methods for characterizing physical properties of nanoparticles are of increasing importance for research and industry. Optical methods are non-invasive and in some cases can be used for routine or in-line applications. The physical parameter which is more often determined is by far the particle size, as this is relevant in determining both the optical and the physical properties. Traditional optical methods for measuring the size of single particles are based on the fundamentals of light scattering, typically the dependence of the scattering cross section C_{sca} upon the particle radius a and the wavelength λ. A tightly focused light beam is usually exploited to maximize the intensity falling onto a single particle, and the scattered intensity (almost isotropic for $a<<\lambda$, barring the dipole term) is collected over a wide solid angle.[1] The ratio between the total scattered power and the incident intensity gives the scattering cross section C_{sca}. Alternatively, the extinction cross section C_{ext}, which gives the total power removed by both scattering and absorption, can be obtained just by measuring the reduction of the incoming light beam when the particle lies across its path. This is done through another class of instruments that is commercially available, the Single Particle Obscuration Sensor (SPOS).[2]

Here we describe a method which gives a measure of the complex amplitude of the forward scattered field *via* a self-reference interferometric scheme in which particles are driven through the focal region of a light beam, and the transmitted light is collected onto a sensor placed in the far field. The method can be used to measure several characteristics of the particles, and in this work we concentrate on the size and refractive index. The advantages of this method with respect to current alternatives are that it is strictly calibration-free and is based on a very simple optical layout. As a particle sizer, it provides high size resolution and allows simultaneous measurement of size and refractive index of single particles. Moreover, results are not affected by polydispersity. In the rest of the paper, we present an analytical model describing the system without any free parameters and show experimental results obtained with calibrated spheres of different materials, comparing the complex fields recovered from the experimental data to rigorous Mie theory calculations. To prove

[a]Author to whom correspondence should be addressed: marco.potenza@unimi.it

the reliability of the system when operating with polydisperse samples, we report experimental results obtained with a suspension of Poly(D,L-lactide-co-glycolide) nanoparticles.

II. SINGLE PARTICLE EXTINCTION AND SCATTERING

For small particles under the Rayleigh approximation the dimensionless scattered field amplitude can be written as[3] $S(0) = ik^3\alpha + \frac{2}{3}k^6\alpha^2$, where α is the polarizability, which is proportional to a^3 and the refractive index mismatch, $(m-1)$. According to the Optical Theorem (OT),[3] the real part of the field gives rise to partially destructive interference with the forward scattered wave which slightly depresses the transmitted power.[3] The *extinction* cross section (i.e. scattering + absorption) is taken into account just from the *forward scattered* field:

$$C_{ext} = C_{sca} + C_{abs} = \frac{4\pi}{k^2} Re\,[S(0)] \tag{1}$$

A key role is played here by the argument of the complex number $S(0)$, *i.e.* the phase lag φ between the scattered and the incoming wave. Eq. (1) shows that the polarizability α is crucial in determining φ, and therefore C_{ext}. It should be noted that absorption cannot be derived from a traditional measurement of the scattered intensity only.

For larger particles, additional terms must be introduced to approximate $S(0)$, and the shape of the particles also plays a role. Exact results can be easily found for spheres through the Mie theory,[3] while the case of non-spherical shapes requires numerical methods.[4] Generally speaking, φ increases with size, eventually saturating for $a>>\lambda$ (the so called diffraction limit). Several methods have previously been developed for measuring φ. Michelson, Mach-Zender and Smartt interferometers were used to get rid of the intense transmitted beam, as accurately described in literature.[5–7] A Nomarskii optical scheme was exploited for measuring the phase change of the whole transmitted wave.[5,6] More recently a simple method for measuring φ for a number of identical scatterers has been suggested,[8] based upon the statistical analysis of the speckle field formed by the superposition of the transmitted and the scattered fields just downstream of the sample. The present method provides the real and imaginary parts of the complex field scattered by single particles through a relatively simple optical layout.

A. Fundamentals of the method

Let a particle be at the centre of the focal region of a light beam. Light is collected at a distance z from the particle in the far field of the beam. The transmitted and scattered wavefronts are concentric, and the Gouy effect shifts the former by $\pi/2$.[9] For a very small particle (φ~0) the two waves are out of phase by $\pi/2$ and the amplitude of the scattered beam is much smaller than the transmitted, so that almost no power is removed by interference.[7] If the particle is displaced along a diameter of the focal spot (say above the optical axis, Fig. 1(a) the wavefronts are slightly skewed.

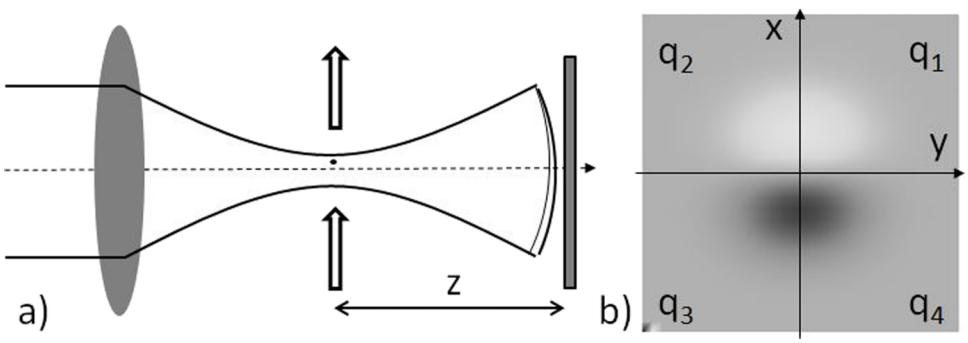

FIG. 1. a) A schematic of the optical layout as described in the text for a very small particle vertically displaced above the optical axis by a distance x_p; b) example of the intensity distribution. The intensity fluctuations are extremely exaggerated.

Interference makes the intensity increase above the optical axis (the two fields add in phase) and decreases it below (they add with opposite phases; Fig. 1(b). The intensity modulation is proportional to the modulus of the scattered field amplitude. Again the overall power is almost unaffected by the presence of the particle. As realized by several authors in the past, a differential measure of the two intensities at opposite sides of the optical axis gives information about either the modulus of the scattered field $s(0)$ or the position of the particle. For example, a sharply focused laser beam was used in connection with optical traps for tracking nano beads, or measuring pico-Newton forces upon them.[10–12] Here we focus on the case of a larger particle, which is much more interesting[5–8] and in connection with our optical scheme represents the main focus of this paper. Let us bring one particle through the focal region, moving along the x axis as indicated by the arrows in Fig. 1(a). For a finite lag φ, the particle at the centre of the focal spot scatters a wave that gives a slightly destructive interference, depressing the main beam power.[7] Accordingly to the OT, this depression accounts for both the scattered and absorbed power, giving rigorously a precise measure of the extinction cross-section C_{ext}. As seen above, if the particle is displaced from the centre of the focal region, the two wavefronts are skewed and the intensity modulation is proportional to is given by the amplitude of the forward scattered field. Hence we propose the name of Single Particle Extinction and Scattering (SPES).

B. Measuring the complex field

From the experimental point of view two main advantages are introduced by the almost perfect matching of the two wavefronts in the far field of the beam: 1) the intensity distribution changes homotetically with the particle-sensor distance z; 2) the intensity modulations occur over wide fractions of the main beam. Sensors with a limited number of elements can then be placed at any distance z, provided that the whole beam is collected. In our experiments we use quadrant photodiodes (QPD), which permit an extended dynamical range and the use of high photocurrent signals, thus making the shot noise negligible. Particles are directed perpendicularly to the optical axis at a constant speed v (some 0.1 m/s) with a concentration that guarantees at most one particle within the focal region (the typical order of magnitude of the concentration used is 10^{-6} particles per cube centimeter). The light falling onto each quadrant is collected and the four fluctuating signals are digitized synchronously at high sampling rates (1 MHz, at least one order of magnitude higher than the inverse transit time), while the total power P of the transmitted beam (5 mW) is continuously monitored by applying a low-pass filter with a time constant $\tau = 250$ μs, much longer than the transit time (of the order of 20 μs).

To give a quantitative description of the system, we now introduce the complex amplitude of the undisturbed field $B(\boldsymbol{r})$ at position $\boldsymbol{r} = (x, y, z)$ onto the sensor plane. For a Gaussian beam with total power P:

$$B(r) = \sqrt{\frac{2P}{\pi}}\frac{1}{w}exp\left[-\frac{x^2+y^2}{w^2}\right]exp\left[-ik\frac{x^2+y^2}{2z}+ikz\right] \tag{2}$$

where w_0 is the beam waist at $z = 0$ and $w{\sim}z\lambda/\pi w_0$ the beam radius at a distance z. The spherical wave scattered by the particle placed at position $(x_p, y_p, 0)$ is:

$$E(r) = \sqrt{\frac{2P}{\pi}}S(0)\frac{1}{kw_0}\frac{1}{iz}exp\left[-\frac{{x_p}^2+{y_p}^2}{w_0^2}\right]\times exp\left[ik\frac{(x-x_p)^2+(y-y_p)^2}{2z}+ikz\right] \tag{3}$$

The intensity is given by $I(x,y) = |B(x,y) + E(x,y)|^2$. The fluctuating component $|B(x,y) + E(x,y)|^2 - |B(x,y)|^2$ can be easily integrated over each portion of the QPD with double integrations from 0 to infinity along x and y. First we consider a particle passing along a diameter of the beam in direction x, *i.e.* for $y_p = 0$. Let be $\xi = \xi(t) = x_p(t)/w_0$. Over the first quadrant $q_1(x, y > 0)$ the power as a function of time is:

$$P_1 = \frac{P}{2}\left(\frac{\lambda}{\pi w_0}\right)^2 s(0)\, e^{-2\xi^2}\,[cos\,\varphi - erfi(\xi)\,sin\,\varphi] \tag{4}$$

Here $S(0) = s(0)\,e^{i\varphi}$, and $erfi\ x = -i\ erf\ (ix)$ is the imaginary error function. Similar results can be obtained for the other three quadrants. The case of the finite sensor size (i.e. using finite integration limits) can also be obtained analytically, and shows that while the sensor is large enough to collect the whole beam, Eq. (4) is valid. By normalizing to the undisturbed beam power P, two parameters can be introduced: 1) the total power attenuation, $A(t) = (P_1 + P_2 + P_3 + P_4)/P$; 2) the intensity *unbalance* generated by interference $U(t) = (P_1 + P_2 - P_3 - P_4)/P$:

$$A(t) = 2\left(\frac{\lambda}{\pi w_0}\right)^2 s(0)\,e^{-2\xi^2(t)}\,cos\varphi \tag{5a}$$

$$U(t) = -2\left(\frac{\lambda}{\pi w_0}\right)^2 s(0)\,e^{-2\xi^2(t)} sin\varphi\ erfi\,\xi(t) \tag{5b}$$

From these expressions it is immediately clear how to recover the real and imaginary parts of $S(0) = s(0)\,e^{i\varphi}$, and hence the amplitude $s(0)$ and the phase φ.

C. Validation of the particle position in the beam

One of the key advantages of the method is allowing the validation of the position of the particle in the middle of the focal region of the beam in an explicit manner. To show how this can be accomplished we introduce the additional parameter $V(t) = (P_1 + P_4 - P_2 - P_3)/P$ and define $= y_p/w_0$, where the particle can pass through the beam at any y_p. We obtain:

$$V(t) = -2\left(\frac{\lambda}{\pi w_0}\right)^2 s(0)\,e^{-2\xi^2(t)} e^{-2\eta^2} sin\varphi\ erfi\,\eta \tag{6}$$

As it can be seen, $V(t)$ vanishes for $y_p = 0$, so that we can rigorously select the signals described by Eq.s (5a) and (5b) that results from particles with y_p~0.

We define t_m the time at which $A(t_m)$ is maximum, that is when the particle is at the centre of the focal region, $(x = 0)$: a negligible $V(t_m)$ guarantees the validity of the condition y_p~0, thus providing an intrinsic validation of the particle position for each signal (see below). We stress that the absence of equivalent validation schemes represents the main limitation of traditional particle counters, for which statistical approaches are often unavoidable.[6]

III. EXPERIMENTAL RESULTS

Fig. 2 shows typical examples of SPES experimental results, obtained for water suspensions of polystyrene (PS) calibrated spheres (a = 215nm; Thermo Scientific 5043A, polydispersity < 3% CV) and a beam waist of 2.1 μm. $A(t)$, $U(t)$ and $V(t)$ are indicated by black circles, open

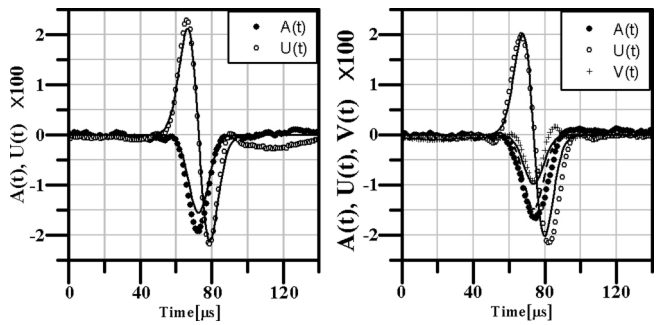

FIG. 2. Examples of signals obtained from PS spheres 215 nm in radius suspended in water, with a waist of 2.1 μm. Left: an example of a particle passed approximately through the center of the beam. Right: signals due to a particle passed at about 100 nm from the center. Solids lines are the expected values obtained from the equations in the text. No free parameter can be introduced to fit curves to data.

circles and crosses respectively. The results expected from Eq.s (5) are shown by solid lines. Fig. 2(a) is for y_p~0 ($V(t)$ is negligible and is not shown). No free parameters are used, except for the time scale that has been fitted to the data. As detailed above, when operating the method, particles can pass at any y_p. Fig. 1(b) presents an example case where we assess from $V(t_m)$ that the particle passed at a distance y_p~100nm from the centre of the focal region. Again, no free parameters are necessary to draw the curves $A(t)$, $U(t)$. Three quantities are measured for each particle: 1) the maximum attenuation, A; 2) the maximum unbalance of $U(t)$, U; 3) the maximum value of $V(t)$, V. Signals with $V<<U$ are selected ($V < 0.2\,U$ has been adopted for the data presented below). The two parameters A and U give $ReS\,(0) = s(0)cos\varphi$ and $ImS\,(0) = s(0)sin\varphi$ respectively, as is evident from Eq.s (5a) and (5b) for $t = t_m$. Notice that no other parameters are required, as λ and w_0 are well known for a given optical setup.

The high sampling rate allows us to reject signals other than those due to single particles passing through the beam waist. Particles passing further than the Rayleigh distance $z_R = \pi\, w_0^2/\lambda$ from the focal plane generate wavefronts which give rise to circular fringes and $A(t)$ and $U(t)$ then show multiple oscillations. When several particles are present within the focal spot multiple peaks are also observed. A pulse shape analysis is therefore very effective in rejecting signals which would give $A(t)$ and $U(t)$ outside the validity limits of Eq.s (5a) and (5b).

The sensitivity of the method can be gauged by changing the beam waist w_0 (see Eq. (4)). Different waists have been tested successfully, from 2.1 up to 15 microns. Current limitations are posed by laser instabilities, which are around 10^{-3} for typical laboratory red lasers. For the differential parameters $U(t)$ and $V(t)$ the noise reduces by approximately an order of magnitude compared to the noise affecting $A(t)$. Even at the highest sampling rates tested, the shot noise were confirmed to be negligible.

Fig. 3 shows SPES results, in terms of $S(0)$ represented in the complex plane, for water suspensions of PS calibrated spheres (a = 145, 215, 300nm; ThermoScientific), PMMA (a = 300nm; Microparticles GMBH) and Ag (a = 50nm; NanoComposix). The plot is a two-dimensional histogram, darker greytones indicating a larger number of particles in any two-dimensional bin. Open circles indicate expected values from Mie theory, also obtained without free parameters. The metallic nature of Ag nanoparticles cause strong absorption, so that light is much more effectively scattered with

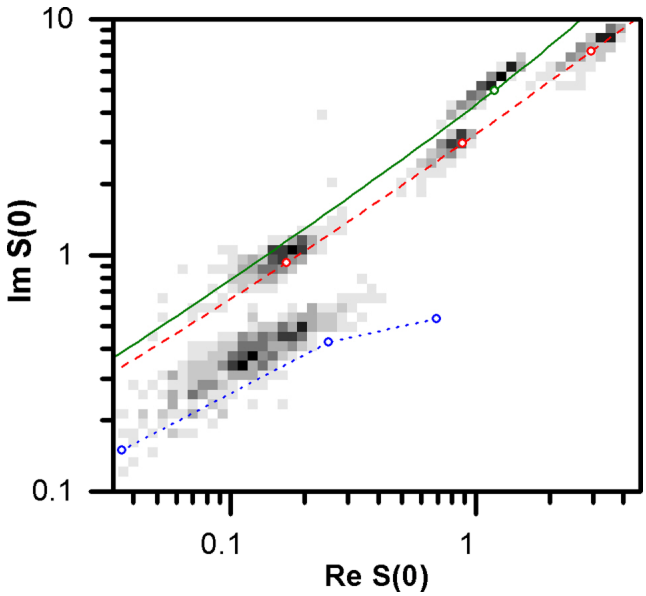

FIG. 3. Experimental results for PMMA, PS and Ag spheres (2D histograms) compared to expected values (open circles) in the complex plane. Lines are just guides to the eye joining the open circles. From top to bottom: PMMA (green, solid line), PS (red, dashed line), Ag (blue, dotted line). For Ag spheres the expected values for 70, 100, 125 nm in diameter have been shown.

respect to dielectric spheres.[2] Although a most complete treatment of the Ag nanospheres case would need to take into consideration the specific plasmonic effects, in order to check the results obtained with Ag we just assumed a tabulated refractive index for Ag nanospheres in water[3] ($m = 0.33 - 3.66i$). By exploiting Mie theory, we get again rough agreement of the SPES data with the expected results, within a factor of 2.

The accuracy of the method can be first evaluated from Fig. 3, by comparing the experimental results with the complex fields calculated for each expected sizes. A better measure of the quality of the results can be obtained by recovering both the refractive indices and sizes for dielectric spheres. Thanks to the single particle detection, a true inversion procedure is not needed here, since each signal can be safely associated with a single size and refractive index. This is rigorously true for dielectric spheres, where these parameters completely fix the scattered complex field. It has been recently shown that the spherical case can be safely exploited for any shape, provided that the particle is not too far from spherical.[14] A proper look up table (LUT) can be easily obtained for a range of refractive indices and a range of sizes on the basis of the rigorous Mie theory. By exploiting the Mie expansion, we have computed the fields scattered by a collection of spheres with refractive index (relative to water) between 1.01 and 1.6, with real and imaginary parts within the ranges 0.1-10 and 0.1-100 respectively. A 75x75 matrix has been obtained by dividing the complex field represented on a log-log scale in uniform rectangular cells. Each cell contains more than one field and is associated with the field which is closer to the center of the cell itself. Finally, each cell is associated with the combination of size and refractive index corresponding to the field. Associating each measured signal $ReS(0)$ and $ImS(0)$ with a given refractive index and size is then straightforward, until the point where effects of Mie resonances introduce oscillations in the complex fields.[3] This is approximately true until $2ka\,(m-1) < 3$, where $k = 2\pi/\lambda$.

Fig. 4 shows the results obtained by applying the LUT to the sets of data corresponding to 600 nm spheres in Fig. 3. Measured refractive indexes relative to water at a wavelength of 635 nm

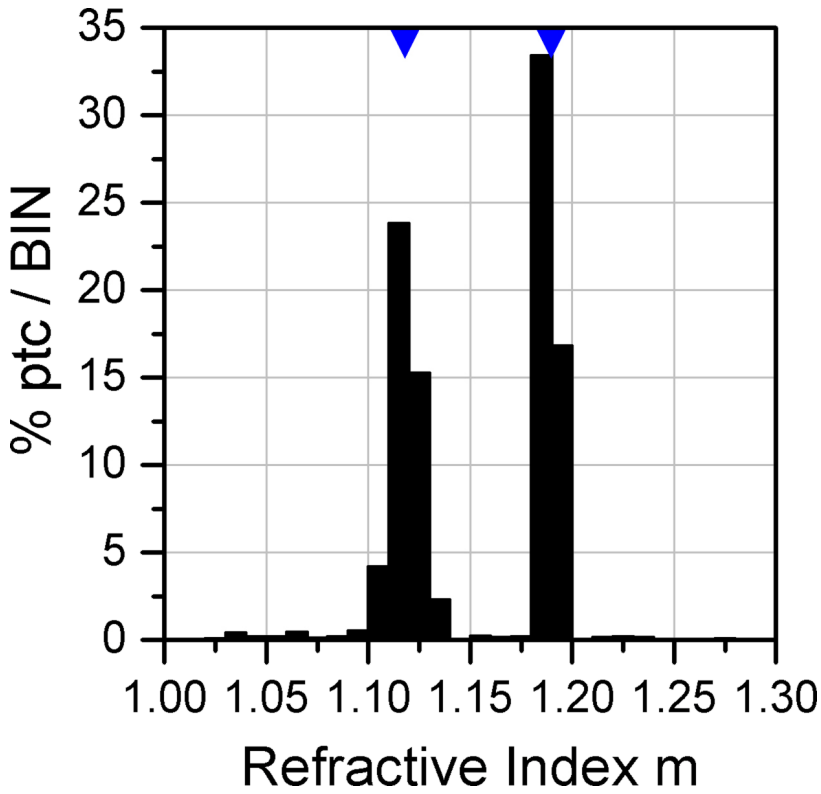

FIG. 4. Refractive index distribution obtained for the PMMA (left) and PS (right) 600 nm spheres reported in Fig. 3. Triangles indicate the expected values.

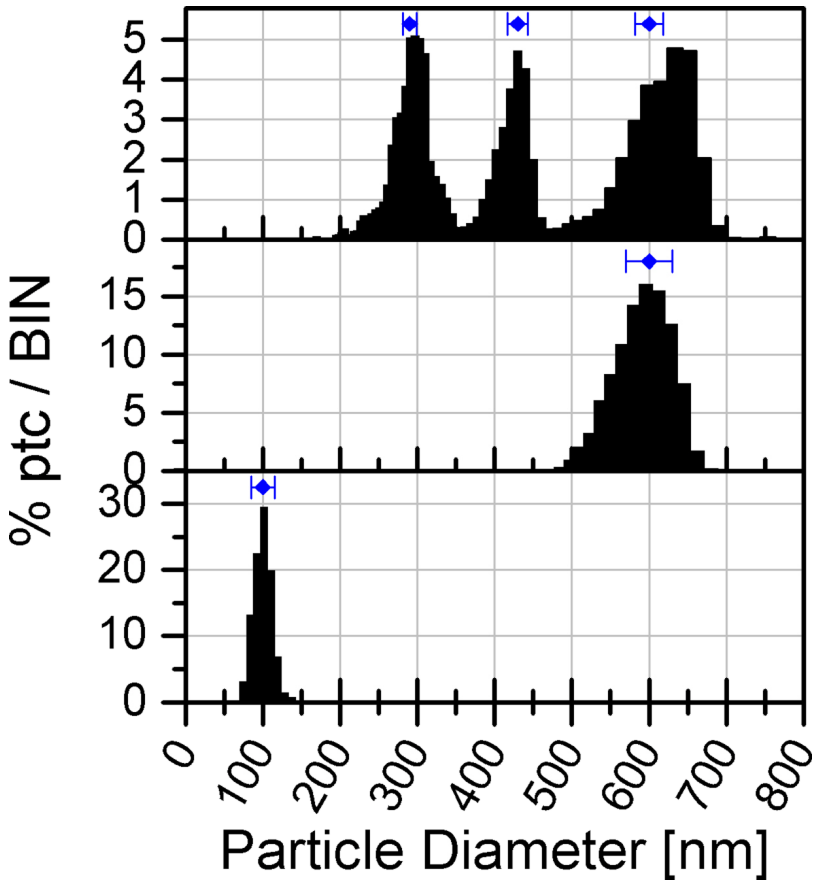

FIG. 5. Particle size distributions as obtained from the experimental results shown in Fig. 3. (a) PS; (b) PMMA; (c) Ag. The same LUT has been used to analyze PS and PMMA. Triangles and horizontal lines respectively indicate the sizes and coefficient of variations reported by the manufacturers.

are 1.118±0.01 and 1.192±0.01, versus the expected 1.12 and 1.19 for PMMA and PS. Notice that the same analysis and LUT cannot be adopted for Ag spheres, because of the imaginary part of the Ag refractive index. In this case a specific, much simpler LUT has been realized (by exploiting Mie theory again, and using the refractive index reported above). In Fig. 5 the particle size distributions are reported for PS (a), PMMA (b) and Ag (c). The average diameters and the coefficients of variation (CV), compared to the nominal values reported by the manufacturers (in parentheses) are reported in Table I. Notice that, thanks to the correct evaluation of the refractive index, the PMMA and PS spheres with a diameter of 600 nm are correctly sized with comparable accuracy and precision, despite the difference in the complex scattered fields being larger than 50%. This would be impossible for any other single particle light scattering method.

TABLE I. Experimental results obtained by sizing calibrated spheres (diameter and coefficient of variation), compared to the nominal values reported by the manufacturers.

Sample	Measured diameter (nm)	Measured CV (%)	Nominal diameter (nm)	Nominal CV (%)
PS 290	288	10	290	3
PS 430	421	6	430	3
PS 600	609	8	600	3
PMMA 600	588	7	600	2.5
Ag 100	101	15	100	<15

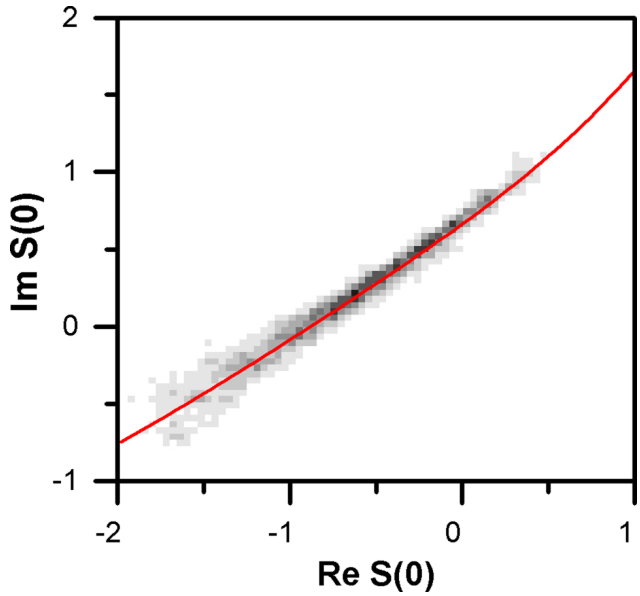

FIG. 6. Experimental results obtained with the water suspension of PLGA nanoparticles. Notice that the population is characterized by a main elongation due to the polydisperse size distribution, and a small spread in the perpendicular direction according to the spherical shape and homogeneity of the particles. Solid line represents the expected values for the fields scattered by spheres with the expected refractive index.

Moreover, the SPES method is robust when operated on polydisperse samples in the single particle detection regime. We support this claim by showing experimental results obtained with a water suspension of Poly(D,L-lactide-co-glycolide) nanospheres. Fig. 6 shows the SPES results represented in a way similar to Fig. 3. The solid line represents the expected values for the fields scattered by spheres with refractive relative to water index m = 1.11. By exploiting once more the LUT for dielectrics we can give a precise characterization of the refractive indexes recovered by the method, which is presented in Fig. 7(a) as a histogram. The blue triangle gives the expected value of the distribution. In Fig. 7(b) we report the size distribution obtained based on SPES measurements and our LUT, which is in accordance with independent measurements by traditional Dynamic Light Scattering.

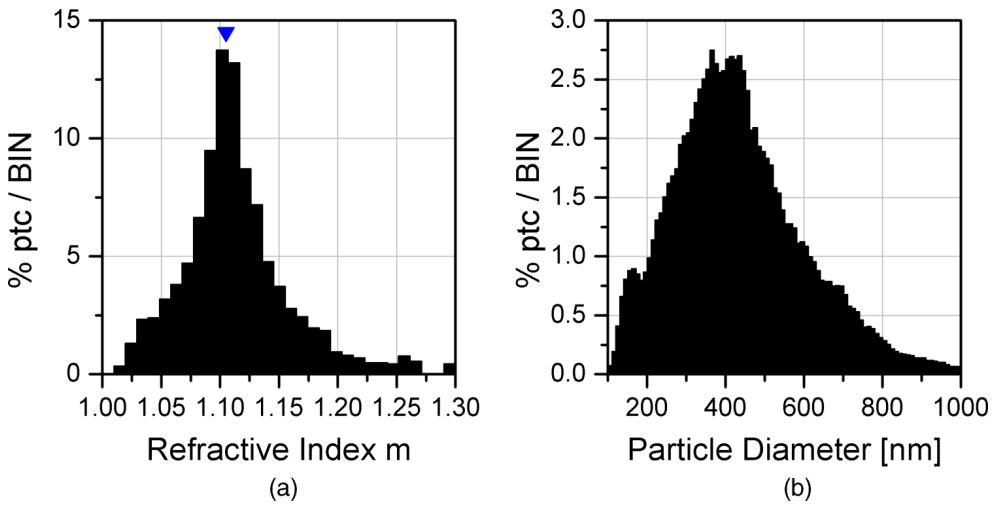

FIG. 7. Refractive index (a) and particle size distribution (b) as obtained from the experimental results reported in Fig. 6. The blue triangle indicates the expected value.

IV. CONCLUSIONS

In conclusion we have described a simple interferometric scheme for measuring the complex scattered field of submicron particles. Accessing two independent parameters such as the real and imaginary parts, or the amplitude and phase, can be of paramount importance for analyzing unknown samples. In particle sizing applications, for example, even with highly polydisperse samples, both the sensitivity and resolution obtained by SPES are higher in comparison with traditional methods. This is mainly due to (in order of importance): 1) the precise estimate of the refractive index, which is essential for recovering the size; 2) the strong validation scheme; 3) the minimal dependence of forward scattering on particle shape.

For these reasons we are convinced that SPES can be exploited well beyond accurate particle sizing applications. In particular, it has been recently shown both theoretically[13] and experimentally[14] that the measurement of the complex field of single particles opens new possibilities for assessing particles features other than size. Nonspherical particles, aggregates of particles, and particles with internal structures can be distinguished from solid, almost spherical particles thanks to the peculiar distributions of $S(0)$ within the complex plane. We stress that one of the most important advantages of the SPES method is that it maintains its performance when operating with highly polydisperse suspensions, which are common in practical applications and represent a major limitation for traditional methods. Moreover, the capability of distinguishing different materials allows to work with complex fluids, such as for example biological fluids. Finally, by exploiting the plasmonic properties of metallic particles in connection with appropriate mathematical modeling,[15] accurate measurements of the complex field will be able to yield important information about the surface: a further unique advantage in comparison to any existing method.

ACKNOWLEDGMENTS

We acknowledge Marzio Giglio for useful discussions, F. Cavaliere and D. Viganò of the Mechanical Workshop of the Physics Department, Simon Brown for accurately reading the manuscript and the anonymous referee for useful suggestions. Marco A.C. Potenza and Tiziano Sanvito declare potential conflict of interest deriving from the exploitation of the SPES method.

[1] P. Chylek *et al.*, Science **193**, 480 (1976).
[2] E.G.M. Pelssers, M.A. Cohen, and G.J. Fleer, J. Colloid Interf. Sci. **137**, 350-361 (1990).
[3] H.C. Van de Hulst, *Light Scattering by Small Particles* (Dover, N.Y, 1981); C.F. Bohren and D.R. Huffmann, *Absorption and Scattering by Small Particles* (Wiley, N.Y, 1983).
[4] M.I. Mishchenko *et al.*, JQSRT **55**, 535 (1996).
[5] J.S. Batchelder and M.A. Taubenblatt, APL **55**, 215 (1989).
[6] J.S. Batchelder and M.A. Taubenblatt, Appl. Opt. **30**, 4972 (1991).
[7] A. Bassini *et al.*, Appl. Opt. **31**, 8121 (1997).
[8] M.A.C. Potenza *et al.*, PRL **105**, 193901 (2010).
[9] M. Born and E. Wolf, *Principles of Optics* (Pergamon, London, 1959).
[10] A. Pralle *et al.*, Micr. Res. And Tech. **44**, 378 (1999).
[11] F.V. Ignatovich and L. Novotny, RSI **74**, 049312 (2003).
[12] F. Gittes and C.F. Schmidt, Opt. Lett **23**, 7 (1998).
[13] M.A.C. Potenza and P. Milani, JNR **16**, 2680 (2014).
[14] M.A.C. Potenza, T. Sanvito, and A. Pullia, JNR **17**, 110 (2015).
[15] R. Saja, private communication.